·Time-dependent fragility functions for circular tunnels in soft soils

Zhongkai Huang[1]; Sotirios Argyroudis[2]; Dongmei Zhang[3]; Kyriazis Pitilakis[4]; Hongwei Huang[5]; Dongming Zhang[6]

1 Postdoctoral Research Fellow, Dept. of Geotechnical Engineering, Tongji Univ., Shanghai 200092, China. ORCID: https://orcid.org/0000-0001-9387-2307. Email: 5huangzhongkai@tongji.edu.cn
2 Assistant Professor, Dept. of Civil and Environmental Engineering, Brunel University London, Uxbridge UB83PH, United Kingdom (corresponding author). ORCID: https://orcid.org/0000-0002-8131-3038. Email: sotirios.argyroudis@brunel.ac.uk
3 Professor, Dept. of Geotechnical Engineering, Tongji Univ., Shanghai 200092, China. Email: dmzhang@tongji.edu.cn
4 Professor, Dept. of Civil Engineering, Aristotle Univ., Thessaloniki, Greece. Email: kpitilak@civil.auth.gr
5 Professor, Dept. of Geotechnical Engineering, Tongji Univ., Shanghai 200092, China. Email: huanghw@tongji.edu.cn
6 Professor, Dept. of Geotechnical Engineering, Tongji Univ., Shanghai 200092, China. Email: 09zhang@tongji.edu.cn

Abstract

Fragility functions are used in the vulnerability analysis of structures considering different sources of uncertainties. In this research, a framework to develop time-dependent fragility functions for circular tunnels embedded in soft soils is proposed, considering the impact of corrosion on the lining reinforcement. Typical shallow and deep circular tunnel sections in soft soils of Shanghai city are used as case studies. The seismic response of the tunnel lining was obtained based on a series of nonlinear dynamic analyses of the soil-tunnel system. The aging effect due to corrosion of the reinforcement bar is considered by decreasing the strength properties of the tunnel lining. Time-dependent fragility curves as a function of free-field peak ground velocity (*PGV*), as well as fragility surfaces in terms of *PGV* and service time *t*, are proposed for minor, moderate and extensive damage states. The main sources of uncertainty are linked with the input motion and frequency content, the soil properties and response, the tunnel embedment depths and the estimation of the damage levels. Results show an overall increase of the seismic fragility for both the shallow and deep tunnels over time, emphasizing the significant impact of aging effects on the performance of tunnels. The findings of this study provide an improved understanding of the performance of tunnels exposed to diverse hazards, and hence, facilitate the life-cycle seismic risk assessment and resilient designs of transport infrastructure.

Author keywords: Circular tunnels; Fragility curves; Fragility surfaces; Damage probability; Aging effects; Numerical study; Soil-structure interaction

Practical Applications

Tunnels are critical assets of the transport infrastructure and provide key services to subway systems of large cities across the globe. During their long life-span, they will be exposed to multiple hazards and exogenous stressors, like earthquakes and corrosion due to ageing, which can lead to failure and disruption of transport operations. Hence, it is of outmost importance to evaluate what is the impact of combined hazard effects in the performance of the tunnels, and to evaluate the likelihood of failure for a range of hazard scenarios. To this end, this study developed novel time-dependent fragility models, which show the probability of exceeding certain damage levels of the structure, for a range of seismic intensities, considering also the deteriorated condition of the structure in different periods after its initial construction, due to chloride induced corrosion of the steel reinforcement. This is applied in circular tunnels sections built in soft soils of Shanghai city. The results clearly indicate that the fragility of tunnels is increased with time, while the fragility is also increased when the overburden height is shorter.

The study highlights the important role of aging effects, tunnel's geometry and embedment and earthquake motion characteristics in the vulnerability of tunnels. The results can support engineers, infrastructure owners and operators, and decision-makers to improve the seismic design of new structures and assess the risks of the aged infrastructure during their life-cycle, and hence to enhance their resilience.

Introduction

Tunnels are a critical component of underground transportation systems in urban areas (Pitilakis et al., 2014; Broere, 2016), while communities in densely populated cities rely upon them (Zhang et al., 2018). However, particular attention should be paid to the structural performance and safety of tunnels in earthquake-prone areas, considering that major damage was observed in underground structures during strong ground shaking in the recent decades (Ghasemi et al., 2000; Wang et al., 2001; Huo et al., 2005; Shimizu et al. 2007). The collapse of Dakai station during the 1995 Kobe earthquake in Japan (Iida et al., 1996) is a rather distinct example, causing the shutdown of the city transportation system and huge economic costs. Therefore, to reduce or even avoid the earthquake-induced damage to tunnel structures, it is of utmost importance to assess their response, fragility and potential risk exposure to a range of seismic intensities. At the same time, underground structures are exposed to water ingress, which in the long term might reduce the strength properties of reinforced concrete (Yang et al., 2019; Mortagi and Ghosh, 2020; Wang, 2021), and hence, increase their vulnerability to seismic hazard.

Fragility curves constitute a powerful tool to evaluate the seismic performance and risk of engineering structures (Baker and Cornell, 2005; Cui et al., 2018; Peña et al., 2019). They provide the probability of reaching or excessing a given damage state under a specific earthquake intensity parameter, while the relevant aleatory and epistemic uncertainties are considered in the probability distribution function for each damage state. Compared to aboveground structures, the research on the seismic fragility of tunnel structures is limited. Up to now, the seismic fragility analysis of tunnels has mainly relied on observation data (ALA, 2001; Corigliano et al., 2007) and expert elicitation approaches (Rojahn and Sharpe, 1985; HAZUS, 2004). More recently, several scholars have proposed a series of fragility functions for different typologies of tunnels and ground conditions using numerical modelling approaches (e.g., Argyroudis and Pitilakis, 2012; Argyroudis et al., 2017; Qiu et al., 2017; Andreotti and Lai, 2019; de Silva et al., 2021). This study contributed to the improved understanding of tunnels' behaviour and reliability under a range of seismic loads, and provided information both for the design process as well as for the risk analysis or stress testing of critical networks subjected to multiple hazards (Argyroudis et al., 2020).

The seismic fragility assessment of tunnel structures is commonly carried out assuming that tunnels are optimally maintained during their life span, while the time-dependent degradation mechanisms adversely affecting their performance are commonly ignored. However, tunnel structures are generally designed to operate for over 100 years, and hence, during their long-life span, the materials of concrete, reinforcement and joint bars are expected to deteriorate, and as a result, the strength of the tunnel lining will be decreased (Yuan et al., 2012; Ai et al., 2016). Particularly, the corrosion of the reinforcing steel is considered as the most common cause of the lining strength deterioration, especially for tunnels located in coastal regions (Gulikers 2003; Zhang and Mansoor, 2013; Bagnoli et al., 2015; He et al., 2019). Moreover, the changing environmental conditions due to global warming and sea-level rise cause an additional increase in the rate of material corrosion (Gao and Wang, 2017; Peng et al., 2017; Mortagi and Ghosh, 2020). To the best knowledge of authors, such kind of aging effect that happens during the life span of tunnels has only been accounted for within a rather limited number of fragility functions (Argyroudis et al., 2017). Furthermore, fragility surfaces, which represent the probability of attaining or excessing a damage level at a specific level of intensity measure and service time of tunnels, have not been proposed in the literature.

The above discussion indicates that further research is required to shed light on this aspect aiming to enhance the understanding of life-cycle seismic risk assessment of tunnels. To this end, the present study proposes a framework to study the potential impact of lining corrosion on the fragility of circular tunnels, as shown in Fig. 1. The organization of the study follows the proposed framework. First, the seismic response of the examined tunnels is evaluated based on detailed numerical modelling, while the derived results are compared with existing analytical solutions (part (a) of Fig. 1). Then, the probabilistic seismic demand models for the as built and deteriorated conditions of the tunnels considering the impact of lining corrosion are generated (part (b) of Fig. 1). Subsequently, time-dependent fragility curves are proposed for the examined tunnels and corrosion conditions, considering different sources of associated uncertainties (part (c) of Fig. 1). Finally, the corresponding fragility surfaces are generated, which can be used to evaluate the tunnel fragilities at any time, in terms of service time and seismic intensity measure (part (d) of Fig. 1). This research highlights the critical factors that significantly influence the seismic fragility of tunnels, i.e. the lining corrosion, tunnel embedment depths and local soil conditions. The outcome of this study facilitates more precise and comprehensive life-cycle seismic fragility and risk assessment of tunnels, and hence, contributes toward more resilient underground transportation systems.

Details of numerical modelling

Tunnel and soil properties

Typical circular tunnels from the metro system of Shanghai city, China are chosen in this research. The tunnel section has an outer diameter d of 6.2 m and a lining thickness q of 0.35 m. To evaluate the impact of the embedment depth on the fragility of the tunnel, two different embedment depths h are chosen, equal to 9 m and 30 m. Thus, the corresponding cover-to outer diameter ratios h/d are equal to 1.45 and 4.84, respectively. They are denoted as shallow and deep tunnels in this study. The other mechanical parameters of the investigated tunnels are shown in Table 1.

Three typical soil profiles are used in this study to consider the variability of soil site conditions in the seismic fragility of tunnels. Fig. 2 shows the detailed soil properties, namely density ρ, shear wave velocity V_s, cohesion c, and friction angle φ for the three soil profiles, represented as D1, D2 and D3, and categorized as soil type D in Eurocode (EC8, 2004) or equivalently site type III or IV based on the Chinese Seismic Design Code (GB50011, 2010). The development of shear modulus G/G_{max} and damping ratio D_r with the shear strain level γ for the clay and sand materials are shown in Fig. 3, which are obtained from the Shanghai issue code for seismic design of underground structures (DG/TJ08-2064-2009, 2010).

Soil-tunnel numerical model

The finite element software Abaqus (2012) is utilized to numerically analyze the complex dynamic behaviour of the soil-tunnel system. Fig. 4 depicts a typical two-dimensional (2D) soil-tunnel numerical model used in this research. The domain of this model is 100 m along the y-direction (vertical direction), and the length of the x-direction (transverse direction) is 400 m. Regarding the modelling of the tunnel lining and to limit the computational cost, two-node beam elements (B21) and a linear elastic model are used. Four node plane strain elements (CPE4R) are utilized to model the soil. The mesh size of the numerical model is properly determined using the suggestions from Lysmer and Kuhlemeyer (1969), to cover the frequency range of interest (0–15 Hz) of the seismic waves used. A so-called finite-sliding hard contact model is utilized to simulate the dynamic behavior of the tunnel-soil interface and facilitate the computation efficiency of the potential nonlinear response. The normal and tangential behavior of interface is simulated by a hard contact formulation and a Coulomb frictional model, respectively. It is noted that the current work did not consider the modelling of the grout layer in the numerical simulations. Determining the thickness, location and actual properties of the grout layer around the circular tunnel is often a complex and case-dependent problem (Zhang et al., 2018). As a result, the potential influence of grouting was often overlooked in previous soil-tunnel dynamic studies (e.g. Tsinidis et al., 2014 and 2016; Zhang et al., 2021).

The accuracy of the numerical results was influenced by the appropriate set of boundary conditions. Consequently, the selection of boundary conditions was critical for the reliable simulation. For the presented study, the boundary conditions are set to avert the negative impact of artificial boundaries on the numerical analysis results. Specifically, the adopted boundary conditions follow the scheme used by many other researchers in relevant studies (Tsinidis et al., 2014, 2016; Andreotti and Lai, 2019; Anato et al., 2021; Zhang et al., 2021), and are validated with centrifuge tests results (Tsinidis et al., 2014, 2015 and 2016). As for the lateral boundaries, horizontal kinematic tie constraints, are set for the nodes on the two vertical sides of the model, so as to allow them to have the same horizontal deformation (Tsinidis et al., 2014). The base of the model is assumed to be the elastic bedrock. Particularly, the infinite extension in depth of the bedrock is modeled using the dashpots (Lysmer and Kuhlemeyer, 1969), and the dashpots coefficients C are determined by the product of the bedrock shear wave velocity V_{sb}, mass density ρ_b and the 'effect area' of each dashpot A.

A widely used elastoplastic Mohr-Coulomb behaviour model was utilized to model the soil behaviour. The parameters of soils are calibrated following the scheme suggested by Pitilakis and Tsinidis (2014). Firstly, the equivalent damping ratio and shear modulus ratio G/G_{max} are evaluated through the 1D ground response analysis by EERA, developed by Bardet et al. (2000). Then, the equivalent soil properties are integrated with a Mohr–Coulomb yield criterion and are further applied in the above-mentioned numerical model.

The numerical analyses, for both the as built and deteriorated conditions of the tunnel, include two steps, i.e. a static step and a dynamic analysis step. First, the soil-tunnel system is analyzed statically, to introduce the geostatic stress in the numerical model, considering the tunnel being in place. Subsequently, the dynamic analyses are conducted, where the earthquake motion is imposed at the base boundary of the numerical model, through the dashpots. The detailed numerical modelling procedure and its validation are described in a previous study (Huang et al., 2020). 2D numerical simulations were adopted to make the computationally intensive nonlinear time-history parametric analysis more efficient. A more rigorous three-dimensional (3D) model, which can capture localized 3D effects, can be employed in future studies.

Selection of the seismic input motions

A representative set of earthquake motions are chosen for the nonlinear soil-tunnel dynamic analysis, to consider the uncertainty in the seismic records, and develop the probabilistic seismic demand model (part b of Fig. 1) for the subsequent fragility analyses of tunnels. The common spectral matching method (Iervolino and Manfredi, 2008) is used to choose the ground motions from the PEER Strong Motion Database (PEER, 2000). A total of 12 real ground motion records are selected and their information is shown in Table 2. The comparison in Fig. 5 indicates that the normalized elastic response spectrum for the chosen ground motions compares well with the relevant design response spectrum from the Chinese Seismic Design Code (GB50011, 2010). The cloud analysis, the incremental dynamic analysis (IDA), and the multiple-stripe analysis are some of the methodologies used in the existing work to investigate the relation between a specified seismic intensity measure (*IM*) and a numerically estimated damage measure (*DM*). The second method, IDA, was used in the present investigation because it covers a large range of ground motion amplitudes, allowing to comprehensively investigate the impact of increasing seismic intensity on the seismic performance of tunnel lining. The amount of input motions needed for IDA is generally determined by the study aims and structural features. According to previous study (Vamvatsikos and Cornell, 2002), a set of ten to twenty true seismic records can cover the epistemic uncertainty in the records while still providing enough accuracy for seismic demand calculations. To analyze the influence of an increasing earthquake intensity on the seismic performance of tunnel lining, a set of twelve real seismic records was chosen, while each ground motion's *PGA* value was scaled from 0.1 to 1.0 g, similarly to other studies (e.g. Di Trapani and Malavisi, 2019; He and Lu, 2019; Miari and Jankowski, 2022). Therefore, a total of 120 scaled ground motions are adopted for the numerical analyses, to develop the fragility functions of the examined tunnels.

Representative numerical results and comparison with analytical solutions

Simplified, yet, well-verified analytical approaches (e.g. Wang, 1993; Penzien, 2000 and Park et al., 2009), are usually applied in the prediction of seismically induced bending moment and axial forces in circular tunnels under plane strain quasi-static conditions at the preliminary design stages of tunnels, owing to their easy calibration and control. Comparisons between numerical dynamic lining forces and these well-known analytical solutions are provided to shed light on the efficiency of the analytical approaches and their discrepancies with the numerical simulations. To use of the above-mentioned analytical solution, the soil shear strain γ_{max} is calculated employing the 2D analysis result as a mean shear strain of the soil computed far away from the tunnel (i.e. "free-field condition") at the same depth with the tunnel centroid. It is noted that only a simple full-slip or no-slip condition is taken into account in the analytical solutions. Herein, the numerical maximum lining forces are calculated by the peak values of the semi-amplitude for cycles in the time series of the so-called steady-state stage (Tsinidis et al., 2014). For all the examined circular tunnels, the soil to tunnel flexibility ratio, i.e. soil-tunnel relative stiffness, F is defined according to Wang (1993):

$$F = \frac{E_s(1-v_l^2)R^3}{6E_l I_l(1+v_s)} \tag{1}$$

where E_s and v_s stand for the soil elastic modulus and Poisson ratio; E_l and v_l are the lining elastic modulus and Poisson ratio; R stands for the radius of the tunnel and I_l represents the inertia of the lining moment (per unit width). Table 3 summarizes calculated flexibility ratios for all the examined soil-tunnel configurations, which range between 2.1 and 10.0, indicating relative flexible tunnels compared with the surrounding soil site.

The comparison between the two approaches for a typical section of the tunnel lining (θ=45°) for the as built conditions of the tunnel in soil type D3 are shown in Fig. 6 and 7, which stand for the results of the shallow and deep tunnel for all seismic input motions, respectively. Fig. 6(a) and Fig. 6(b) contrast the numerically predicted dynamic bending moments and the corresponding results by the analytical solutions, the latter referring to the conditions of full-slip or no-slip interface. For both full-slip and no-slip conditions, it is found that at low seismic intensities (i.e. for *PGA* values up to 0.3g) the comparisons are in good agreement, whereas at high input intensities, the numerically derived bending moments are observed to be significantly lower compared to those resulted by the analytical solutions. Additionally, the three adopted analytical solutions present similar results for conditions of full-slip interface, whereas for no-slip conditions, the analytical predictions according to Wang (1993) are slightly higher than Penzien (2000), whereas, Park et al. (2009) predictions are slightly lower than that of Penzien (2000). The above conclusions are consistent with the findings by Hashash et al. (2001), Kontoe et al. (2011, 2014) and Argyroudis et al. (2017).

Fig. 6(c) and Fig. 6(d) show the comparisons between numerically derived dynamic axial forces and the corresponding analytical predictions using full-slip and no-slip conditions, respectively. For the conditions of full-slip interface, as shown in Fig. 6(c), it is observed that the numerically derived bending moments are generally higher than those obtained from the analytical approaches, while all the analytical predictions are identical with each other. On the contrary, for no-slip conditions, as shown in Fig. 6(d), most analytical predictions are higher than the numerical results apart from the Penzien (2000) solution under low input intensities, which are much closer to the numerical results. Moreover, the dynamic axial forces are significantly underestimated by the Penzien (2000) solution, compared with Wang (1993) and Park et al. (2009) predictions under no-slip conditions. The abovementioned phenomena are also reported by other researchers in relevant studies (Kontoe et al., 2011, 2014; Argyroudis et al., 2017). Similar conclusions can be drawn for the comparisons of dynamic lining forces for the deep tunnels, as presented in Fig. 7.

The above observations demonstrate that these widely used analytical solutions may significantly underestimate or overestimate the dynamic lining forces, indicating that they should be used with utmost caution in engineering practice, while a relatively sophisticated nonlinear dynamic numerical analyses is suggested, so as to obtain more precise results. Generally, compared with the numerical simulations, these analytical solutions suppose an elastic behaviour for the surrounding soil, simple full-slip or no-slip conditions and statically imposed shear wave loading. Moreover, the analytical solutions cannot consider the redistribution of stresses in the vicinity of the tunnel structure, due to soil yielding and nonlinear behavior of the soil-tunnel interface, and their impacts on the dynamic lining forces. This discussion explains the observed discrepancies between the analytical and the full numerical results to some extent.

Time-dependent seismic fragility analyses

Definition of damage states

The choice of a clearly-defined damage measure (*DM*) constitutes a priority factor to quantitatively determine the damage state (*ds*) of tunnels. The *DM* adopted in this study is determined using a ratio of the actual (M) over the capacity (M_{Rd}) bending moment for the tunnel lining section, as shown in the following equation:

$$DM = M/M_{Rd} \quad (2)$$

This *DM* was introduced by Argyroudis and Pitilakis (2012), and is widely used in the fragility assessment of tunnels. In this study, it is noted that the acting bending moment (*M*) is computed by applying a combination of geostatic and seismic loads, with the latter defined at the specific time point, as the tunnel exhibits maximum ovaling deformation (Argyroudis et al., 2017). The capacity (M_{Rd}) bending moment can be calculated using the geometry and material properties of the examined tunnel lining, through a section analysis using code FAGUS (Cubus, 2002) with the assumption of the lining behaving like a beam section. The influence of corrosion of reinforcement bar on the lining capacity is also taken into consideration at this step. According to the previous study (Argyroudis and Pitilakis, 2012), five damage states are finally utilized in terms of *DM*, standing for the exceedance of none, minor, moderate, extensive and collapse damage for the tunnels, they are further shown in Table 4.

Definition of fragility curves

The vulnerability of structures can be commonly assessed using fragility functions (Shinozuka et al., 2000; Gardoni et al., 2003). The two-parameter lognormal distribution function is widely used for the development of the fragility functions because of the simple parametric form (Shinozuka et al., 2000; Choi et al., 2004; Cui et al., 2018; Fotopoulou et al., 2018) and is also adopted in this study. This function can be described by the following equation:

$$P[ds \geq ds_i | IM] = \Phi \left[\frac{In(IM)\text{-}In(IM_{mi})}{\beta_{tot}} \right] \quad (3)$$

where $P(\bullet)$ represents the probability of reaching or excessing a determined damage state ds_i under a specific *IM*, which is expressed in terms of peak ground velocity *PGV* in this work according to the recommendations of Huang et al. (2021). Φ stands for the standard normal cumulative distribution function. IM_{mi} represents the corresponding mean value of *PGV* at which tunnels reach the i_{th} damage state. β_{tot} stands for the total standard deviation and can be further computed as follows in Eq. 4, considering associated uncertainties:

$$\beta_{tot}=\sqrt{\beta_C^2+\beta_D^2+\beta_{ds}^2} \tag{4}$$

The parameter β_{ds} represents the epistemic uncertainty associated with the limitation in the calculation of the damage states by the definition of *DM*, and is assumed equal to 0.3 (Argyroudis and Pitilakis, 2012). The parameter β_C is the aleatory uncertainty associated with the definition of the capacity of the lining of the studied tunnels and is set equal to 0.4 according to HAZUS (2004). It should be highlighted that the consideration of uncertainties in fragility assessment is a major challenge, and in some cases it relies on simplified assumptions (Selva et al., 2013; Sevieri et al., 2020). For different geotechnical components, different values of β_{ds} and β_C have been used (Argyroudis et al. 2019). To the authors' best knowledge, the uncertainty from the threshold values of the damage states β_{ds} and the capacity β_C of tunnels have not yet been explored thoroughly, and therefore more work using experimental, numerical and monitoring methods is required. β_{ds} is commonly in the range of 0.20 to 0.71 (Argyroudis et al. 2019), with an average of 0.4 being used for tunnels (Huang et al. 2017; Argyroudis et al. 2019). Furthermore, the capacity β_C's uncertainty is typically between 0.14 and 0.50 (Argyroudis et al. 2019), whereas for tunnels, a value of 0.3 is commonly supposed according to engineering judgment (Selva et al., 2013; de Silva et al. 2021). Due to a lack of related research and a more rigorous prediction way, the selected values of β_{ds} and β_C in this work are compatible with earlier similar investigations (de Silva et al. 2021; Shekhar and Ghosh, 2021). Parameter β_D stands for the aleatory uncertainty related to the earthquake input motions, the frequency content of the seismic input used in the numerical simulation and the corresponding variability in the soil response. This parameter is calculated as the mean standard deviation of the *IM–DM* (in logarithmic scale) regression analysis. Therefore, the primary sources of uncertainties in the seismic demand as well as the structural capacity are considered in this study (Silva et al., 2019), including the variability in the input motion, the soil properties and response, the tunnel embedment depths and the definition of damage levels. The integration of these uncertainties leads to more accurate seismic fragility analysis results.

Consideration of lining corrosion

Corrosion causes the direct loss of the cross-sectional area for the reinforcement bar and results in a decline of the tunnel lining strength in the long operation life (Ai et al., 2016). Although some models that describe the corrosion mechanisms of reinforced concrete (RC) structures are existing (e.g. Enright and Frangopol, 1998; Vu and Stewart, 2000; He et al., 2019), to the authors' best knowledge, similar approaches that reveal the corrosion effect on the tunnel lining strength are currently not available. In this regard, the consideration of lining corrosion in this study follows the modelling employed by Argyroudis et al. (2017). This simplified time-dependent corrosion modeling method is also widely-used in the seismic fragility analysis of aging bridge structures (Akiyama et al., 2011; Ai et al., 2016; Rao et al., 2017; Deng et al., 2018). Therefore, to accurately assess the time-dependent seismic response of tunnel lining subjected to corrosion effects, more rigorous constitutive models of steel reinforcement and concrete should be developed in the future, based on experimental and theoretical results.

Specifically, the chloride-induced corrosion of reinforcement bars is generally recognized as one of the most severe and common degradation phenomenon for RC structures. Corrosion initiation time T_0 plays a vital role in the degradation model of lining reinforcement bars according to Fick's second law. Herein, the the corrosion initiation time T_0 is expressed by the model introduced by CEB-FIB-Task Group 5.6 (2006):

$$T_0 = \left(\frac{a^2}{4 \times k_e \times k_t \times D_{RCM,0} \times (t_0)^n} \times \left(erf^{-1}(1 - \frac{C_{crit}}{C_S}) \right)^{-2} \right)^{(\frac{1}{1-n})} \quad (5)$$

where α is the thickness of the concrete (mm), k_e represents an environmental function, k_t stands for the transfer variable, $D_{RCM,0}$= chloride migration coefficient (m^2/s), t_0 stands for the reference point of time (years), n represents the aging exponent, *erf* stands for the Gaussian error function; C_{crit} stands for the critical chloride content and C_s is the equilibrium chloride concentration at the concrete surface, these two parameter can be defined by a percentage by weight of cement (*wt* % cement).

This work adopts an assumption that the corrosion will develop uniformly along the perimeter of a reinforcing bar. Hence, the time-dependent cross-sectional area $A(t)$ of lining reinforcement bars can be calculated utilizing this equation (e.g. Ghosh and Padgett, 2010):

$$A(t) = \begin{cases} k \times D_0^2 \times \dfrac{\pi}{4} & t < T_0 \\ k \times (D(\mathrm{t}))^2 \times \dfrac{\pi}{4} & T_0 \le t \end{cases} \tag{6}$$

where $A(t)$ is the time-dependent bar cross-sectional area, k stands for the amount of reinforcing bars, D_0 represents the original diameter of reinforcement bar, t stands for the time (in years) since the operational start of the tunnel, and $D(t)$ represents the diameter of the corroded bar at the service time of t, which can be calculated using this equation:

$$D(t) = D_0 - i_{corr} \times \varphi \times (t - T_0) \tag{7}$$

where i_{corr} stands for the parameter of corrosion rate (mA/cm^2), and φ represents the corrosion penetration (μm/year).

Table 5 presents the adopted values of the model parameters describing the chloride-induced corrosion in this study. It is noted that the values of these parameters can refer to the recommendations of FIB-CEB Task Group 5.6 (2006) and some relevant research (e.g. Stewart, 2004; Choe et al., 2008, 2009). Moreover, for the examined chloride-induced degradation case herein, an assumption of a “submerged” exposure environment (e.g. k_e=0.325, Choe et al., 2008, 2009; Ghosh and Padgett, 2010) is made, its corresponding water-to cement ratio of the concrete material is 0.5. The above degradation scenario is realistic for tunnels or other underground infrastructures (Choe et al., 2009). It should be mentioned that the used corrosion rate (i_{cor}=7 mA/cm^2) indicates a relatively high corrosion intensity (Stewart, 2004) and is assumed to be constant over the service life of the structures (Ghosh and Padgett, 2010).

Based on the above methodology, the corrosion initiation time can be calculated and is equal to 20.7 years, while the bar area loss is calculated for various tunnel operation years *t*. For the studied tunnel cases, the bar area loss is defined for three different scenarios, i.e. t= 50, 75, 100 years, and given in Table 6.

The *DMs* for the as built and deteriorated conditions of the tunnel were derived using the following procedures. For the scenario before the corrosion initiation (t<20.7 years), a series of numerical simulations were conducted, and the *DM* is calculated directly based on the dynamical responses of tunnel lining in this case. While for the other aging scenarios (i.e. *t* equal to 50, 75, 100 years), firstly, the reinforcement of tunnel lining was modified based on the above-mentioned methodology (Eq. 4), through the modification of bar area for different operation time *t*. Then, the degradation of the capacity (M_{Rd}) bending moment for tunnel lining section could be calculated using section analysis, and thus the time-dependent *DM* for the considered tunnels can be calculated for the fragility analyses.

Development of probabilistic seismic demand model

The probabilistic seismic demand model constitutes the basis for the fragility analysis of structures (Gardoni et al., 2003). Generally, it can be obtained through the regression analysis between damage measure (*DM*) and earthquake intensity (*IM*) (part (b) of Fig. 1) (Freddi et al., 2017). Taking the scenario of initial (as built) conditions (t=0 year) and the aging scenario t= 50 years as examples, Fig. 8(a) and Fig. 8(b) present the plots (in the natural logarithm scale) of the derived *DM-PGV* relationships for the examined shallow and deep tunnels in soil type D, which represents the sum up of the three soil profiles in a single soil profile. The different dots show the calculated data for *DM* under various input intensities, while the blue solid line indicates the regression fit curve for these damage measure data. Through this procedure, IM_{mi} can be calculated according to the regression fit equation based on the different thresholds of damage states. The uncertainty owing to the seismic demand β_D can be computed according to the dispersion of the simulated *DMs* with regard to the predicted *DMs* from the regression fitted model, while the total variability β_{tot} is estimated using Eq. 4.

Following the above approach, for different considered aging scenario t= 0, 50, 75 and 100 years, the corresponding fragility function parameters, i.e. the median (IM_{mi}) and standard deviation (β_{tot}), can be obtained and they are summarized in Table 7 and 8 for shallow and deep tunnels, respectively.

Development of fragility curves

Based on the derived fragility function parameters for shallow and deep tunnels (Table 7 and 8) in the examined soil type, the computed novel fragility curves as a function of *PGV* at the surface for different aging scenarios (t=0, 50, 75 and 100 years) are given in Fig. 9 and Fig. 10, respectively. Generally, for the same aging scenario and seismic intensity measure level, it is found that the computed fragility of the shallow tunnels generally is larger than the deep tunnels. This finding is in agreement with previous studies (Cilingir et al., 2011; Chen et al., 2012). With the increase of *PGV*, the damage probability of the tunnel is increased for all three damage states. The results show that both shallow and deep tunnels are quite safe under low earthquake excitations (typically PGV<0.3 m/s). However, under very strong earthquake excitations (typically PGV>0.8 m/s), it is noted that shallow tunnels have a high possibility to undergo extensive damage, while deep tunnels are rather safe, although it is expected to undergo minor or moderate damage to some degree. These results show the vital role of tunnel embedment depths in the fragility analysis of tunnel structures.

Furthermore, the seismic fragility of both the shallow and deep tunnels will increase significantly as the service time t increases, because of the aging effects. As an illustrative case, for the PGV = 0.5 m/s and in the scenario of the shallow tunnel, the exceedance probability of damage for initial conditions (t= 0 year) is equal to 0.692, 0.171 and 0.014 for minor, moderate and extensive damage, respectively. However, for the corrosion scenario of 50 years, the exceedance probability will be increased to 0.882, 0.375 and 0.053 for minor, moderate and extensive damage, respectively. Thus, for above three damage states, the exceedance probability for the aging scenario of 50 years will be increased on average by 14.4%. Accounting for the aging scenario of 100 years, the exceedance probabilities are equal to 0.994, 0.850 and 0.402, for minor, moderate and extensive damage, respectively. This indicates that the exceedance probability will be increased in average by 45.6% for the three damage states. Similar results are also found for the case of the deep tunnel. Therefore, it is evident that ignoring the lining corrosion in the design and risk analysis of tunnels will result in an underestimation of structural fragilities. These results highlight the critical effect of lining corrosion on the fragility of tunnels.

For the case of deep tunnels, a comparison between the empirical fragility functions developed by Corigliano et al. (2007) as a function of *PGV*, and the generated ones by the work for initial conditions (t=0 year) and the service time of 100 years, is shown in Fig. 11. It is noted that no empirical curves are provided for extensive damage for the deep tunnel, thus only the curves in terms of minor and moderate damage are adopted for the comparison. Moreover, the empirical fragility curves by Corigliano et al. (2007) were generated using 120 cases of earthquake-related damages from past earthquakes in variable soil conditions, while this study adopts a numerical-based approach. Therefore, the comparison herein is generally qualitative but is still useful for a better understanding of the fragility assessment of tunnels. Significant discrepancies are found between the numerical and empirical fragility curves, considering that the examined tunnel typologies, the tunnel service time, soil conditions, as well as the procedure to derive the fragility curves are different between the two approaches. Nevertheless, the comparison in Fig. 11 highlights the important role of aging effects, tunnel typology as well as soil conditions on the seismic fragility estimates of tunnels.

Development of time-dependent fragility surfaces

The definition of fragility parameters for different time points in service life of tunnels is essential to continuously obtain the time-dependent seismic fragility. To this end, analytical functions representing time-dependent fragility models constitute a powerful tool for estimating the fragility parameters at any point in time without the requirement to carry out additional numerical analyses. Based on the study of Gosh and Padgett (2010), the following equation, which is modified from Eq. 3, can be used to evaluate the tunnel fragilities at any time after the initial construction, as:

$$P_f(IM,t) = \Phi\left[\frac{1}{\beta_{tot}(t)} \cdot In(\frac{IM}{IM_{mi}(t)})\right] = \Phi\left[\frac{1}{a_1 t^2 + a_2 t + a_3} \cdot In(\frac{IM}{b_1 t^2 + b_2 t + b_3})\right] \tag{8}$$

where the coefficients of a_1, a_2 and a_3 indicate the dispersion β_{tot}, while the coefficients of b_1, b_2 and b_3 indicate the median threshold value of IM_{mi} for a given damage state. These coefficients can be further determined through the regression analysis using the datasets from Table 6 and Table 7. Table 9 summarizes the coefficients for the fragility parameters for three damage states of the considered tunnels in soil type D.

Based on Eq. 8 and the corresponding coefficients in Table 9, the fragility surfaces in terms of service time *t* and *PGV* for shallow and deep tunnels in soil type D are produced, as shown in Fig. 12 and Fig. 13. These surfaces provide a more comprehensive assessment of the fragility and expected losses for increasing service time of the infrastructure. Based on these plots, the seismic fragility of both the shallow and deep tunnels increases significantly over time due to aging (i.e. corrosion) effects. The increase of fragility is more apparent for the shallow tunnel and the extensive damage state. The developed fragility surfaces in Fig. 12 and Fig. 13 can be used to evaluate the vulnerability of tunnels at any point in service time, which can facilitate the quantitative life-cycle seismic risk analysis of tunnels in similar soil sites.

Conclusions

This study developed novel time-dependent fragility functions of circular tunnels constructed in soft soils exposed to ground shaking. Critical factors influencing the seismic performance and fragility of circular tunnels, including the aging effect due to the corrosion of the lining reinforcement, the tunnel embedment depths and the earthquake motion characteristics, were thoroughly examined. The seismic performance of the tunnel lining was assessed based on numerous 2D nonlinear dynamic analyses under variable earthquake intensities. The probabilistic seismic demand models were then generated to estimate the parameters of fragility function. Time-dependent fragility functions were proposed for different levels of PGV at the surface, and fragility surfaces in terms of service time t and PGV at the surface were also developed. From the obtained results, it is evident that the fragility of tunnels would increase with time, because of the degradation of the tunnel lining capacity caused by its reinforcement corrosion, while the fragility is also increased when the tunnel embedment depth is smaller. This highlights the important role of aging effects, tunnel embedment depths and earthquake motion characteristics in the fragility of tunnels subjected to seismic loading.

The proposed time-dependent fragility curves, and the corresponding fragility surfaces, could be utilized in the quantitative life-cycle seismic risk assessment of tunnels in similar soil conditions. Future studies can include the time-variant corrosion rate in the analysis, accounting for the influential factor of climate change projections, which can exacerbate the water and chloride ingress in concrete structures. More advanced models can be developed to reflect the corrosion mechanisms of underground structures based on laboratory tests, considering the uncertainties from the corrosion development and structural properties of the grouting layer, to improve life-cycle fragility assessments.

Data Availability Statement

All of the data, models, or code that support the findings of this study are available from the corresponding author upon reasonable request.

Acknowledgements

This work is sponsored by National Natural Science Foundation of China (Grants No. 52108381,41772295, 51978517, 52090082), Shanghai Science and Technology Committee Program (Grants No. 21DZ1200601, 20DZ1201404), Innovation Program of Shanghai Municipal Education Commission (Grant No. 2019-01-07-00-07-456 E00051), National Key Research and Development Program of China（Grant No. 2021YFF0502200) and China Postdoctoral Science Foundation (Grant No. 2021M702491).

References

ABAQUS, 2012. "Users Manual V. 6.12-1." Providence, RI: Dassault Systemes Simulia Corp, USA.

Ai, Q., Y. Yuan, S. Mahadevan, and X. Jiang. 2016. "Probabilistic degradation modelling of circular tunnels assembled from segmental linings." *Struct. Concr.* 17(2): 257-273.

Akiyama, M., D. M. Frangopol, and H. Matsuzaki. 2011. "Life-cycle reliability of RC bridge piers under seismic and airborne chloride hazards." *Earthq. Eng. Struct. Dyn.* 40 (15): 1671–1687.

ALA (American Lifelines Alliance). 2001. *Seismic fragility formulations for water systems part 1 guideline*. Washington, DC.

Anato, N. J., O. C. Assogba, A. Tang, and D. Youssouf. 2021. "Numerical investigation of seismic isolation layer performance for tunnel lining in Shanghai soft ground." *Arabian J. Sci. Eng.* 46(11), 11355-11372.

Andreotti, G., and C. G. Lai, 2019. "Use of fragility curves to assess the seismic vulnerability in the risk analysis of mountain tunnels. " *Tunn. Undergr. Space Technol.* 91, 103008.

Argyroudis, S., A. Mitoulis, G. Winter, and A.M. Kaynia. 2019. "Fragility of transport assets exposed to multiple hazards: State-of-the-art review toward infrastructural resilience." *Reliab. Eng. Syst. Saf.* 191: 106567.

Argyroudis, S. A., et al. 2020. "A risk-based multi-level stress test methodology: Application to six critical non-nuclear infrastructures in Europe." *Nat. Hazards* 100(2): 595–633.

Argyroudis, S., and K. Pitilakis. 2012. "Seismic fragility curves of shallow tunnels in alluvial deposits." *Soil Dyn. Earthq. Eng.* 35: 1–12.

Argyroudis, S., G. Tsinidis, F. Gatti, and K. Pitilakis. 2017. "Effects of SSI and lining corrosion on the seismic vulnerability of shallow circular tunnels." *Soil Dyn. Earthq. Eng.* 98: 244–256.

Bagnoli, P., M. Bonfanti, G. Della Vecchia, M. Lualdi, and L. Sgambi. 2015. "A method to estimate concrete hydraulic conductivity of underground tunnel to assess lining degradation." *Tunn. Undergr. Space Technol.* 50: 415-423.

Baker, J. W., and C. A. Cornell. 2005. "A vector valued ground motion intensity measure consisting of spectral acceleration and epsilon." *Earthq Eng Struct Dyn*. 34 (10): 1193–217.

Bardet, J. P., K. Ichii, and C. H. Lin. 2000. *EERA*. *A computer program for Equivalent-linear Earthquake site Response Analyses of layered soil deposits*, University of Southern California, Department of Civil Engineering, Los Angeles, Calif.

Broere, W. 2016. "Urban underground space: Solving the problems of today's cities." *Tunn. Undergr. Space*

Technol. 55 (May): 245–248.

CEB-FIB Task Group 5.6. 2006. Model for service life design. fédération internationale dubéton (fib).

Chen, C. H., T. T. Wang, F. S. Jeng, and T. H. Huang. 2012. “Mechanisms causing seismic damage of tunnels at different depths.” *Tunn. Undergr. Space Technol.* 28: 31-40.

Choe, D. E., P. Gardoni, D. Rosowsky, and T. Haukaas. 2008. “Probabilistic capacity models and seismic fragility estimates for RC columns subject to corrosion.” *Reliab. Eng. Syst. Safe*. 93(3):383–393.

Choe, D. E., P. Gardoni, D. Rosowsky, and T. Haukaas. 2009. “Seismic fragility estimates for reinforced concrete bridges subject to corrosion.” *Struct. Safety* 31(4):275–283.

Choi, E., R. DesRoches, and B. Nielson. 2004. “Seismic fragility of typical bridges in moderate seismic zones.” *Eng. Struct.* 26(2): 187-199.

Cui, F., H.Zhang, M. Ghosn, and Y. Xu. 2018. “Seismic fragility analysis of deteriorating RC bridge substructures subject to marine chloride-induced corrosion.” *Eng. Struct.*155:61-72.

Cilingir, U., and S. P. G. Madabhushi. 2011. “A model study on the effects of input motion on the seismic behavior of tunnels.” *Soil Dyn. Earthq. Eng.* 31: 452–462.

Corigliano, M., C.G. Lai, and G. Barla. (2007). “Seismic vulnerability of rock tunnels using fragility curves.” *Proc., 11th Congress of the Intern Society for Rock Mech*, Taylor & Francis, Lisbon, Portugal, 1173–1176.

Deng, P., C. Zhang, S. Pei, and Z. Jin. 2018. “Modeling the impact of corrosion on seismic performance of multi-span simply-supported bridges.” *Constr. Build. Mater.* 185 (Oct): 193–205.

de Silva, F., S. Fabozzi, N. Nikitas, E. Bilotta, and R. Fuentes. 2021. “Seismic vulnerability of circular tunnels in sand.” *Géotechnique*. 71(11): 1056–1070.

Di Trapani, F., M. Malavisi. 2019. “Seismic fragility assessment of infilled frames subject to mainshock/aftershock sequences using a double incremental dynamic analysis approach.” *Bull. Earthq. Eng.* 17(1): 211-235.

DG/TJ08-2064-2009. Tongji University. 2010. *Code for Seismic Design of Subway Structures, Shanghai Urban Constructions Communications*. Beijing: China Planning Press.

EC8, 2004. Eurocode 8: Design of Structures for Earthquake Resistance. The European Standard EN 1998-1, Brussels, Belgium.

Enright M.P., and D.M. Frangopol. 1998. “Probabilistic analysis of resistance degradation of reinforced concrete bridge beams under corrosion.” *Eng. Struct.* 20(11): 960–71.

Fotopoulou, S., S. Karafagka, and K. Pitilakis. 2018. “Vulnerability assessment of low-code reinforced concrete frame buildings subjected to liquefaction-induced differential displacements.” *Soil Dyn. Earthq. Eng.* 110: 173–84.

Freddi, F., J. E. Padgett, and A. Dall’Asta, 2017. “Probabilistic seismic demand modeling of local level response parameters of an RC frame.” *Bull. Earthq. Eng*. 15(1), 1-23.

Gao, X. J., and X. Y. Wang. 2017. “Impacts of global warming and sea level rise on service life of chloride-exposed concrete structures.” *Sustainability*, 9(3): 460.

Gardoni, P., K. M. Mosalam, and A. Der Kiureghian. 2003. “Probabilistic seismic demand models and fragility estimates for RC bridges.” J. Earthq. Eng. 7(spec01): 79-106.

GB50011-2010. China Ministry of Housing and Urban-Rural Development. 2016. *Code for Seismic Design of Buildings*. Beijing: China Architecture and Building Press.

Ghasemi, H., J. D. Cooper, R. Imbsen, H. Piskin, F. Inal, and A. Tiras. 2000. “The November 1999 Duzce Earthquake: Post-Earthquake Investigation of the Structures in the TEM.” *Publication No. FHwA-RD00-146*, U.S. Dept. of Transportation, Federal Highway Administration, Washington, D.C.

Ghosh, J., and J. E. Padgett. 2010. “Aging considerations in the development of time-dependent seismic fragility curves.” *J. Struct. Eng.* 136(12): 1497-1511.

Gulikers, J. 2003. “Problems encountered in the detection of reinforcement corrosion in concrete tunnel linings–theoretical considerations.” *Mater. Corro* .54(6): 454-459.

Hashash, Y. M., J. J. Hook, B. Schmidt, I. John, and C. Yao. 2001. “Seismic design and analysis of underground structures.” *Tunn. Undergr. Space Technol.* 16: 247–293.

HAZUS-MH. 2003. Multi-hazard loss estimation methodology: Earthquake model. Washington, DC: Dept. of Homeland Security, FEMA

He, X., Z. Lu. 2019. “Seismic fragility assessment of a super tall building with hybrid control strategy using IDA method.” *Soil Dyn. Earthq. Eng.* 123: 278-291.

He, Z. S., M. Akiyama, C. He, D. M. Frangopol, and S. J. Liu. 2019. “Life-cycle reliability analysis of shield tunnels in coastal regions: emphasis on flexural performance of deteriorating segmental linings.” *Struct. Infrastruct. Eng.* 15(7): 851-871.

Huang, G., W. Qiu, and J. Zhang. 2017. “Modelling seismic fragility of a rock mountain tunnel based on support vector machine.” *Soil Dyn. Earthq. Eng.* 102: 160–171.

Huang, Z. K., K. Pitilakis, S. Argyroudis, G. Tsinidis, and D. M. Zhang. 2021. “Selection of optimal intensity measures for fragility assessment of circular tunnels in soft soil deposits.” *Soil Dyn. Earthq. Eng.* 145(9).

Huang, Z. K., K. Pitilakis, G. Tsinidis, S. Argyroudis, and D. M. Zhang. 2020. “Seismic vulnerability of circular tunnels in soft soil deposits: The case of Shanghai metropolitan system.” *Tunn. Undergr. Space Technol.* 98: 103341.

Huo, H., A. Bobet, G. Fern´andez, and J. Ramírez. 2005. “Load transfer mechanisms between underground structure and surrounding ground: evaluation of the failure of the failure of the Daikai station.” *J. Geotech. Geoenviron. Eng.* 131 (12): 1522–1533.

Iervolino, I., and G. Manfredi. 2008. *A review of ground motion record selection strategies for dynamic structural analysis.* Vienna: Springer.

Iida, H., T. Hiroto, N. Yoshida, and M. Iwafuji. 1996. “Damage to Daikai subway station.” *Soils Found*. Special Issue: 283–300.

Kontoe, S., V. Avgerinos, and D. M. Potts. 2014. “Numerical validation of analytical solutions and their use for equivalent-linear seismic analysis of circular tunnels.” *Soil Dyn. Earthq. Eng.* 66: 206-219.

Kontoe, S., L. Zdravkovic, D. M. Potts, and C. Mentiki. 2011. “On the relative merits of simple and advanced constitutive models in dynamic analysis of tunnels.” *Geotechnique.* 61 (10): 815–829.

Lysmer, J., and R. L. Kuhlemeyer. 1969. “Finite dynamic model for infinite media.” *J. Eng. Mech. Div.,* ASCE, 95(4): 859–878.

Miari, M., R. Jankowski. 2022. “Incremental dynamic analysis and fragility assessment of buildings founded on different soil types experiencing structural pounding during earthquakes.” *Eng. Struct.* 252: 113118.

Mortagi, M., and J. Ghosh. 2020. “Climate change considerations for seismic vulnerability assessment of aging highway bridges.” *ASCE-ASME J. Risk Uncertainty Eng. Syst. Part A: Civ. Eng.* 6 (1): 04020005.

Pacific Earthquake Engineering Research Center (PEER). 2000. *PEER Strong Motion Database*. Berkeley, CA: University of California, Berkeley.

Park, K. H., K. Tantayopin, B. Tontavanich, and A. Owatsiriwong. 2009. “Analytical solution for seismic-induced ovaling of circular tunnel lining under no-slip interface conditions: a revisit.” *Tunn. Undergr. Space Technol.* 24(2):231–235.

Peña, F., I. Bilionis, and S. Dyke. 2019. “Model selection and uncertainty quantification of seismic fragility functions.” *ASCE-ASME J. Risk Uncertainty Eng. Syst. Part A: Civ. Eng.* 5(3): 04019009.

Peng, L., M. G. Stewart, and R. E. Melchers. 2017. "Corrosion and capacity prediction of marine steel infrastructure under a changing environment." *Struct. Infrastruct. Eng.* 13(8): 988-1001.

Penzien, J. 2000. "Seismically induced racking of tunnel linings." *Earthq Eng Struct Dyn*. 29: 683–91.

Pitilakis, K., and G. Tsinidis. 2014. "Performance and seismic design of underground structures." *Earthquake geotechnical engineering design*, Springer, 279-340.

Pitilakis, K., Crowley, H. and Kaynia, A. 2014. *SYNER-G: typology definition and fragility functions for physical elements at seismic risk*. Springer Dordrecht Netherlands.

Qiu, W., G. Huang, H. Zhou, and W. Xu. 2018. "Seismic vulnerability analysis of rock mountain tunnel." *Int. J. Geomech.* 18(3): 04018002.

Rao, A. S., M. D. Lepech, A. S. Kiremidjian, and X.Y. Sun. 2017. "Simplified structural deterioration model for reinforced concrete bridge piers under cyclic loading." *Struct. Infrastruct. Eng.* 13 (1): 55–66.

Rojahn, C., and R. L. Sharpe. 1985. "Earthquake damage evaluation data for California." *ATC-13*. Redwood City, CA: Applied Technology Council.

Selva, J., S.A. Argyroudis, and K. Pitilakis. 2013. "Impact on loss/risk assessments of inter-model variability in vulnerability analysis. " *Nat. hazard.* 67(2): 723-746.

Sevieri, G., A. De Falco, and G. Marmo. 2020. "Shedding light on the effect of uncertainties in the seismic fragility analysis of existing concrete dams." *Infrastruct*. 5(3): 22.

Shekhar, S., and J. Ghosh. 2021. "Improved component-level deterioration modeling and capacity estimation for seismic fragility assessment of highway bridges." *ASCE-ASME J. Risk Uncertainty Eng. Syst. Part A: Civ. Eng.* 7(4): 04021053.

Shimizu, M., T. Saito, A. Suzuki, and T. Asakura. 2007. "Results of survey regarding damages of railroad tunnels caused by the Mid Niigata Prefecture Earthquake in 2004." *Tunneling Underground.* 38 (4): 265–273.

Shinozuka, M., M. Q. Feng, H. K. Kim, and S. H. Kim. 2000. "Nonlinear static procedure for fragility curve development." *J. Eng. Mech*. 126(12): 1287-1295.

Silva, V., et al. 2019. "Current challenges and future trends in analytical fragility and vulnerability modeling." *Earthq. Spectra.* 35(4), 1927-1952.

Stewart, M. G. 2004. "Spatial variability of pitting corrosion and its influence on structural fragility and reliability of RC beams in flexure." *Struct. Saf.* 26(4): 453-470.

Tsinidis, G., K. Pitilakis, and A. D. Trikalioti. 2014. "Numerical simulation of round robin numerical test on tunnels using a simplified kinematic hardening model." *Acta Geotech.* 9(4): 641–659.

Tsinidis, G., K. Pitilakis, G. Madabhushi, and C. Heron. 2015. "Dynamic response of flexible square tunnels: centrifuge testing and validation of existing design methodologies." *Geotechnique*. 65(5), 401-417.

Tsinidis, G., K. Pitilakis, and G. Madabhushi. 2016. "On the dynamic response of square tunnels in sand." *Eng. Struct.* 125, 419-437.

Vamvatsikos, D., C.A. Cornell. 2002. "Incremental dynamic analysis." *Earthquake Eng. Struct. Dyn.* 31:491-514.

Vu K.A.T., and M.G. Stewart. 2000. "Structural reliability of concrete bridges including improved chloride-induced corrosion models." *Struct. Saf.* 22(4): 313–333.

Wang J. N. 1993. *Seismic design of tunnels: a simple state of the art design approach.* New York: Parsons Brinckerhoff.

Wang, C. 2021. "Reliability-based design of lining structures for underground space against water seepage." *Undergr. Space*. 6(3): 290-299.

Wang, W. L., T. T. Wang, J. J. Su, C. H. Lin, C. R. Seng, and T. H. Huang. 2001. "Assessment of damage in mountain tunnels due to the Taiwan Chi-Chi Earthquake." *Tunn. Undergr. Space Technol.* 16(3): 133–150.

Yang, W., C. Q. Li, and H. Baji. (2019). "Design for service life of underground space based on water seepage criterion." *Tunn. Undergr. Space Technol.* 93: 10306.

Yuan, Y., Y. Bai, and J. Liu. 2012. "Assessment service state of tunnel structure." *Tunn. Undergr. Space Technol.* 27(1): 72-85.

Zhang, C., M. Zhao, Z. Zhong, and X Du. 2021. "Seismic intensity measures and fragility analysis for subway stations subjected to near-fault ground motions with velocity pulses." *J. Earthquake Eng.* 1-27.

Zhang, D. M., Z. K. Huang, R. L. Wang, J. Y. Yan, and J. Zhang. 2018. "Grouting-based treatment of tunnel settlement: Practice in Shanghai." *Tunn. Undergr. Space Technol.* 80: 181–196.

Zhang, Z. Q., and Y. A. Mansoor. 2013. "Evaluating the strength of corroded tunnel lining under limiting corrosion conditions." *Tunn. Undergr. Space Technol.* 38: 464-475.

List of Tables

Table 1. Mechanical parameters of the examined tunnel sections.

Parameters	Adopted value
Embedment depth, h (m)	9.0, 30.0
Bending reinforcement, A_s (cm^2/m)	21.0, 58.0
Tunnel outer diameter, d (m)	6.2
Lining thickness, q (m)	0.35
Concrete elastic modulus, E_c (Gpa)	3.55
Concrete Poisson ratio, v_c	0.2
Steel elastic modulus, E_s (Gpa)	200
Steel Poisson ratio, v_s	0.2
Concrete cover depth of lining, c (cm)	5.0

Table 2. Lists of records used for the numerical simulations (*PGA*: peak ground acceleration, *Mag.*: Moment magnitude, *R*: epicentral distance).

Earthquake (Year)	Station name	*PGA* (g)	*Mag.* (M_w)	*R* (km)
Tottori, Japan (2000)	TTR008	0.39	6.61	6.86
Northridge USA (1994)	LA - Hollywood Stor FF	0.23	6.69	19.73
Parkfield, USA (1966)	Cholame-Shandon Array	0.24	6.19	12.90
Imperial Valley-07, USA (1979)	El Centro Array #11	0.19	5.01	13.61
Superstition Hills-01, USA (1987)	Imperial Valley W.L. Array	0.13	6.22	17.59
Imperial Valley-02, USA (1940)	El Centro Array #9	0.28	6.95	6.09
Kobe, Japan (1995)	Port Island	0.32	6.90	3.31
Parkfield-02, USA (2004)	Parkfield-Cholame 2WA	0.62	6.00	1.63
Borrego Mtn, USA (1968)	El Centro Array #9	0.16	6.63	45.12
Loma Prieta, USA (1989)	Treasure Island	0.16	6.93	77.32
Kern County, USA (1952)	Taft Lincoln School	0.15	7.36	38.42
San Fernando, USA (1971)	Castaic - Old Ridge Route	0.34	6.61	19.33

Table 3. Computed flexibility ratios for the examined tunnel-soil configurations.

Tunnel type	Soil type D1	Soil type D2	Soil type D3
Shallow tunnel	2.1	2.7	4.1
Deep tunnel	6.3	9.0	10.0

Table 4. Definition of various damage states of tunnel lining.

Damage state (ds_i)	Range of damage measure (DM)	Central value of DM
ds_0. None damage	$DM \leq 1.0$	-
ds_1. Minor damage	$1.0 < DM \leq 1.5$	1.25
ds_2. Moderate damage	$1.5 < DM \leq 2.5$	2.00
ds_3. Extensive damage	$2.5 < DM \leq 3.5$	3.00
ds_4. Collapse	$DM \geq 3.5$	-

Table 5. Mean values of parameters impacting the chloride-induced corrosion degradation of RC structures.

Parameters	Value	References
Cover depth α (cm)	5.0	-
Environmental transfer variable *ke*	0.325	Choe et al. (2008)
Chloride migration coefficient $D_{RCM,0}$ (m^{2}/s)	8.9e-^{12}	CEB-FIB Task Group 5.6 (2006)
Aging exponent *n*	0.3	CEB-FIB Task Group 5.6 (2006)
Critical chloride concentration (C_{cr}) *wt*% cement	0.6	CEB-FIB Task Group 5.6 (2006)
Surface chloride concentration (C_s) *wt*% cement	4.5	Choe et al. (2009)
Rate of corrosion (i_{corr}) mA/cm^2	7.0	High corrosion intensity (Stewart, 2004)

Table 6. Bar area reduction (%) of various aging scenarios.

t（year）	50	75	100
Shallow tunnel	27.5	47.5	64.3
Deep tunnel	18.8	33.4	46.5

Table 7. Derived fragility function parameters (*PGV* in m/s and total standard deviation β_{tot}) for shallow tunnel in as built (t=0) and different aging scenarios (t= 50, 75, 100 years).

t（year）	Minor (m/s)	Moderate (m/s)	Extensive (m/s)	β_{tot}
t=0	0.381	0.838	1.652	0.543
t=50	0.260	0.596	1.218	0.551
t=75	0.187	0.431	0.883	0.555
t=100	0.133	0.308	0.632	0.560

Table 8. Derived fragility function parameters (*PGV* in m/s and total standard deviation β_{tot}) for deep tunnel in as built (t=0) and different aging scenarios (t= 50, 75, 100 years).

t（year）	Minor (m/s)	Moderate (m/s)	Extensive (m/s)	β_{tot}
t=0	0.833	1.694	3.124	0.529
t=50	0.688	1.397	2.574	0.528
t=75	0.582	1.180	2.170	0.530
t=100	0.489	0.989	1.817	0.529

Table 9. Coefficients for the fragility surfaces of the examined tunnels.

Tunnels and damage states		$IM_{mi}(t)$			$\beta_{tot}(t)$		
Tunnel typology	Damage states	b_1	b_2	b_3	a_1	a_2	a_3
Shallow tunnel	Minor	2E-5	-0.005	0.483	-8E-7	3E-4	0.537
	Moderate	3E-5	-0.010	1.042			
	Extensive	4E -5	-0.018	2.013			
Deep tunnel	Minor	1E -5	-0.006	0.947	6E-8	-3E-8	0.529
	Moderate	2E -5	-0.012	1.927			
	Extensive	4E -5	-0.022	3.556			

List of Figures

Fig. 12. Fragility surfaces in terms of service time *t* and *PGV* for the shallow tunnel in soil type D. (a) Minor damage; (b) Moderate damage; (c) Extensive damage.

Fig. 13. Fragility surfaces in terms of service time *t* and *PGV* for the deep tunnel in soil type D. (a) Minor damage; (b) Moderate damage; (c) Extensive damage.

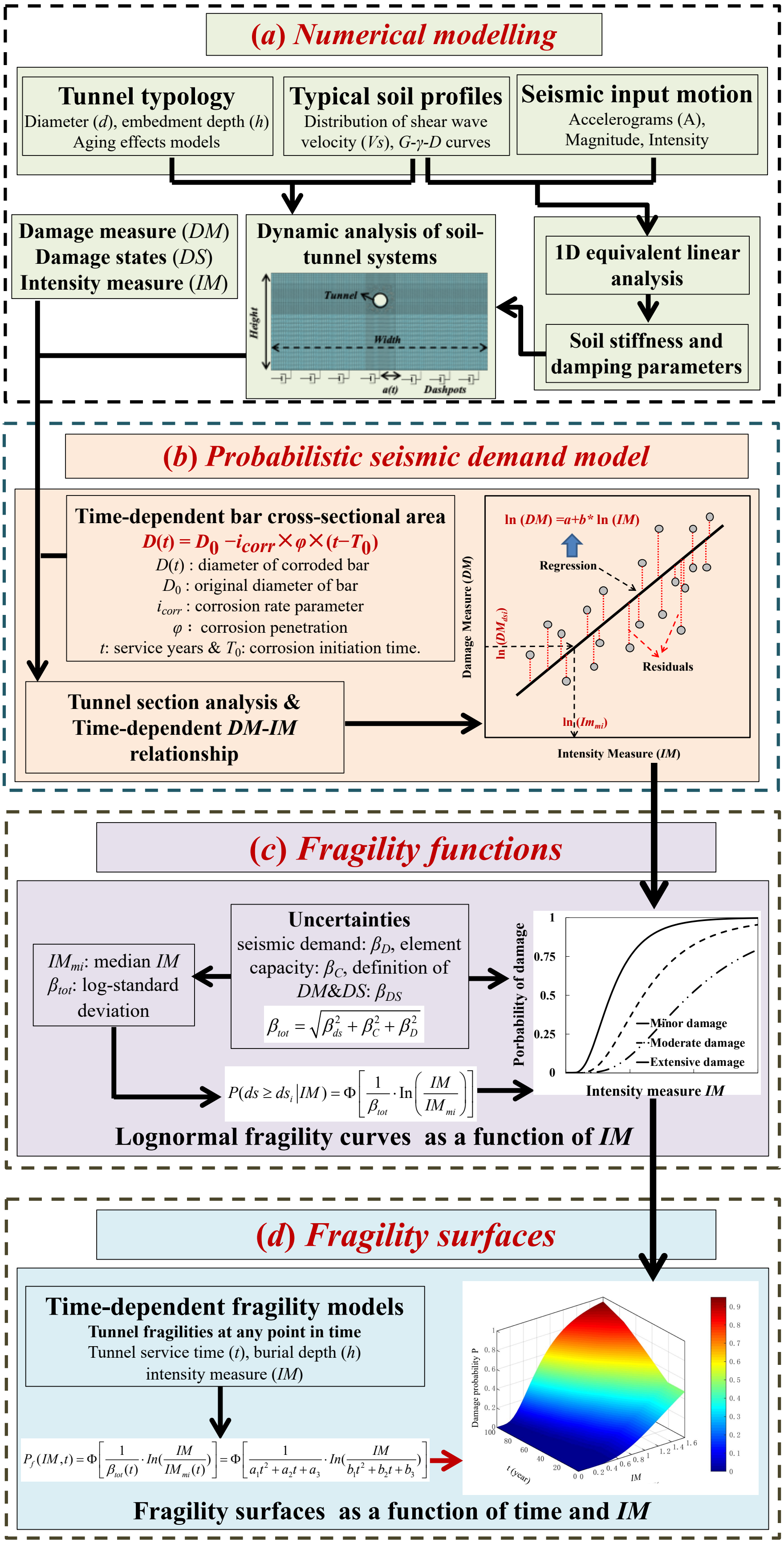

Fig. 1. Proposed framework for the construction of time-dependent fragility functions for tunnels.

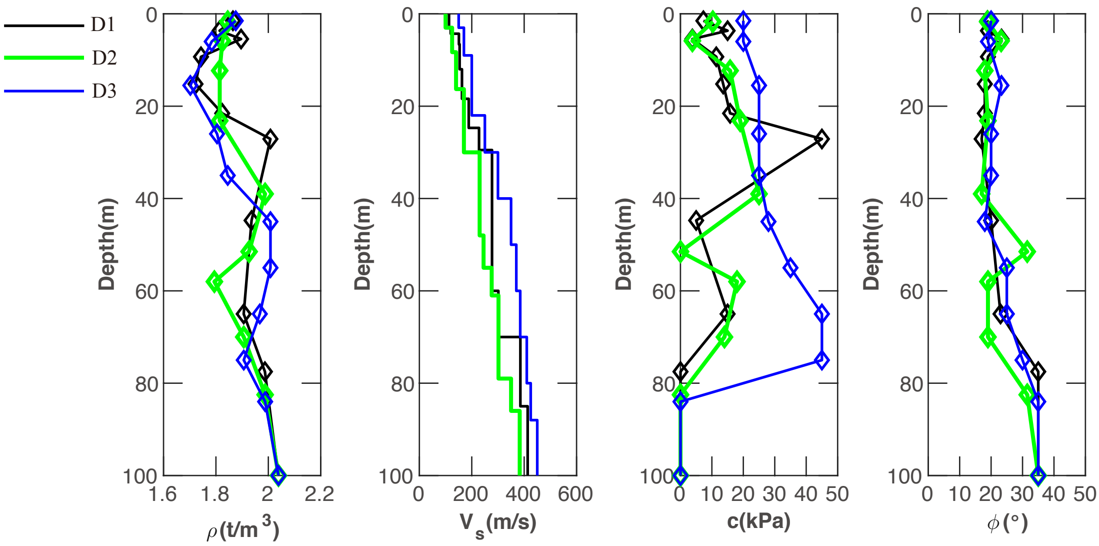

Fig. 2. Typical geotechnical properties of the soil profiles.

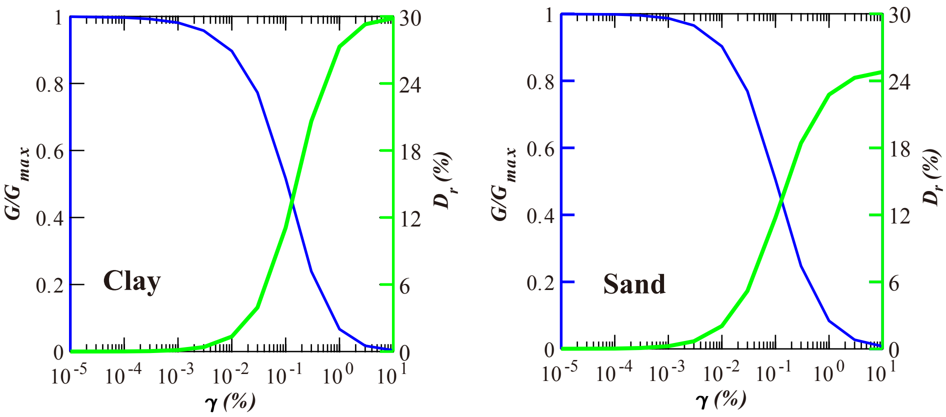

Fig. 3. Typical G-γ-D_r curves used for clay and sand in the examined soil deposits.

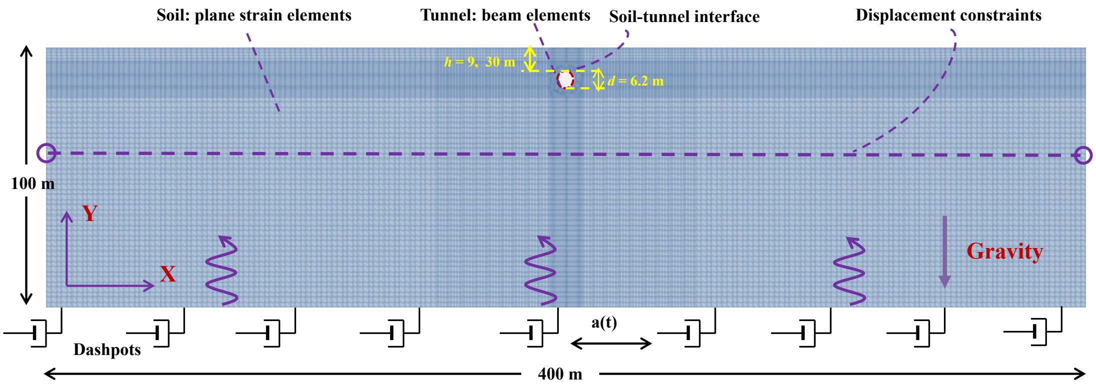

Fig. 4. 2D view and the mesh of the numerical model.

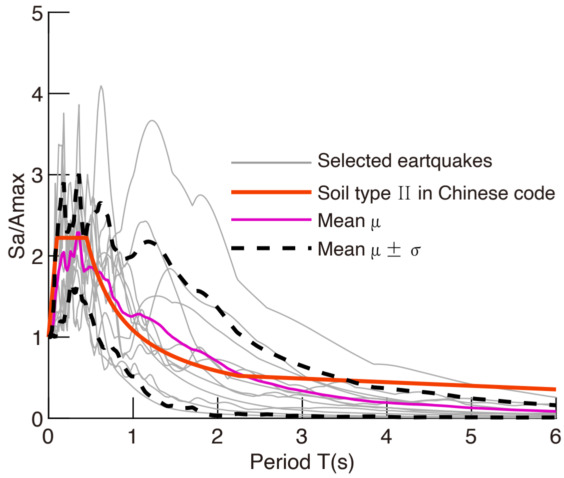

Fig. 5. Comparison of the normalized elastic response spectrum of the input motions with the corresponding design spectrum from the Chinese seismic code (GB50011, 2010).

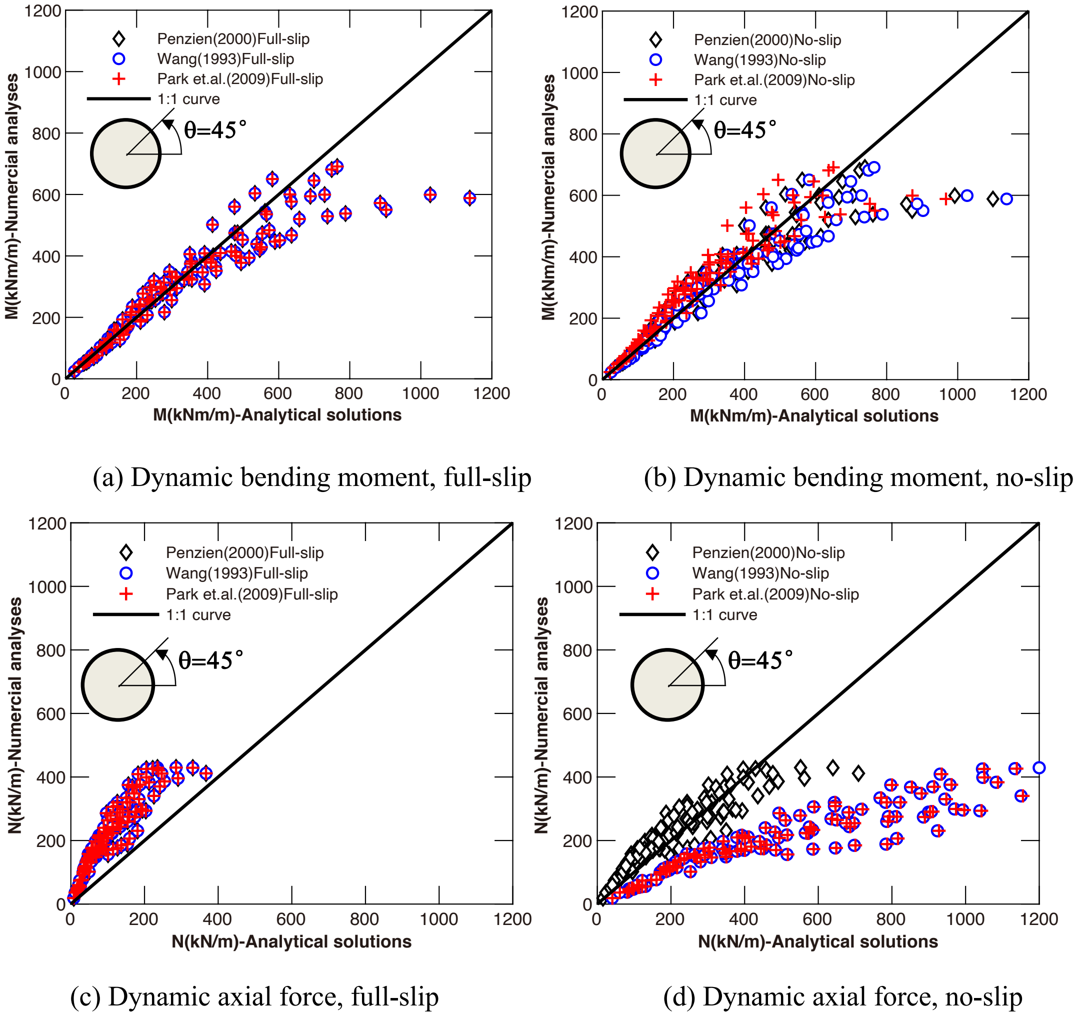

(a) Dynamic bending moment, full-slip (b) Dynamic bending moment, no-slip

(c) Dynamic axial force, full-slip (d) Dynamic axial force, no-slip

Fig.6. Comparisons of numerically and analytically predicted dynamic lining forces of a critical lining section (θ=45°) of shallow tunnel in soil type D3. (a) Dynamic bending moment, full-slip; (b) Dynamic bending moment, no-slip;(c) Dynamic axial force, full-slip; (d) Dynamic axial force, no-slip.

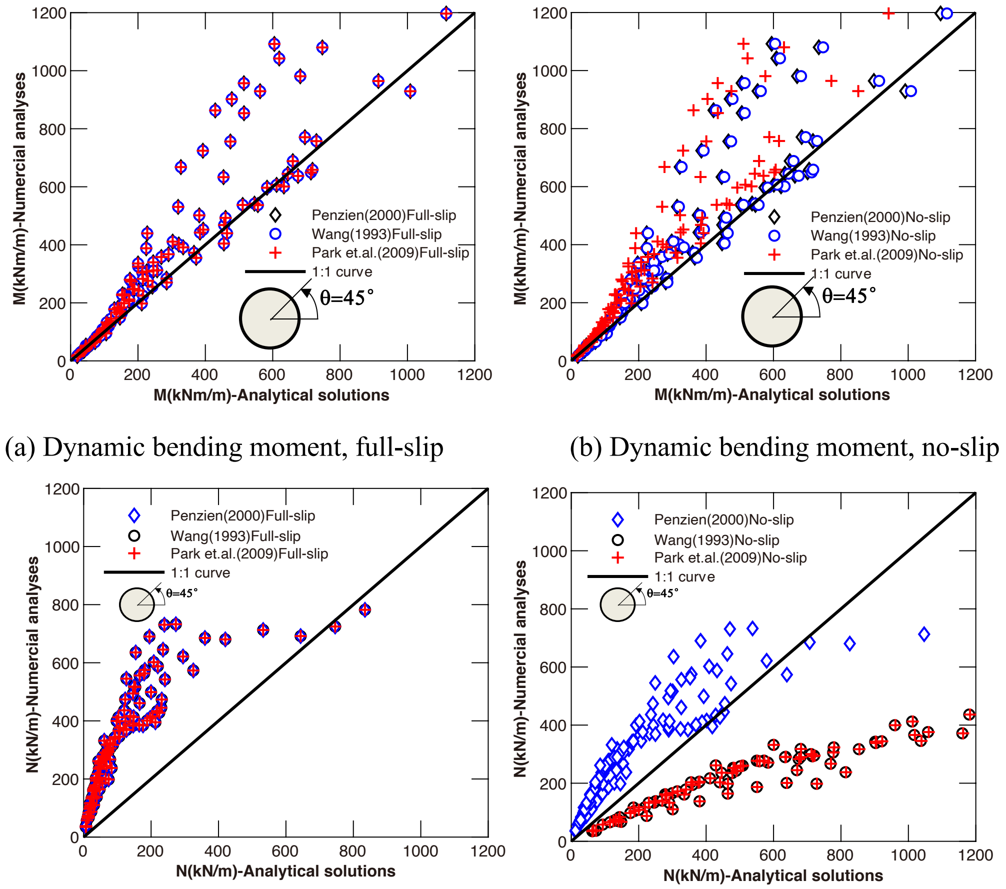

(a) Dynamic bending moment, full-slip

(b) Dynamic bending moment, no-slip

(c) Dynamic axial force, full-slip

(d) Dynamic axial force, no-slip

Fig.7. Comparisons of numerically and analytically predicted dynamic lining forces of a critical lining section (θ=45°) of deep tunnel in soil type D3. (a) Dynamic bending moment, full-slip; (b) Dynamic bending moment, no-slip;(c) Dynamic axial force, full-slip; (d) Dynamic axial force, no-slip.

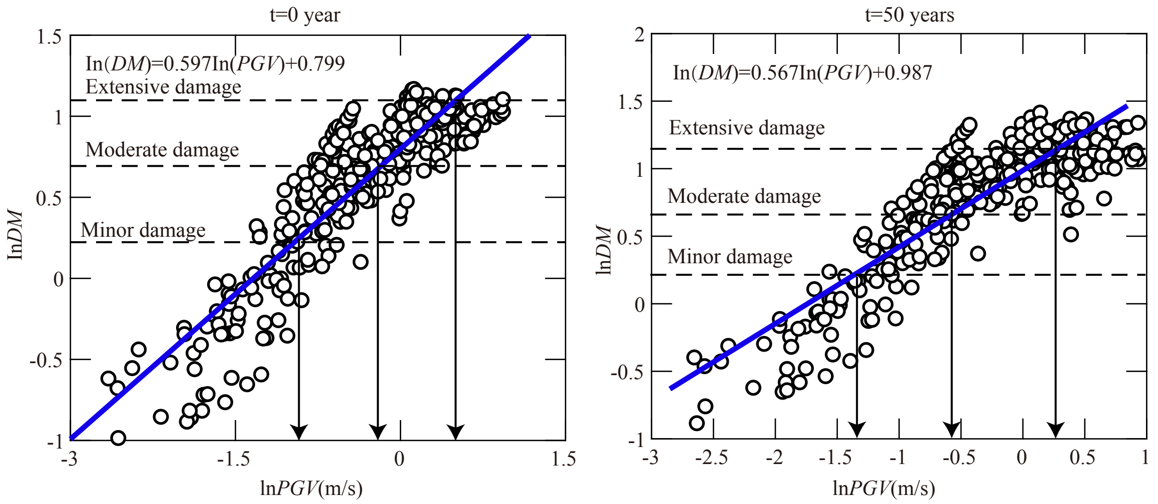

(a) Shallow tunnel in soil type D

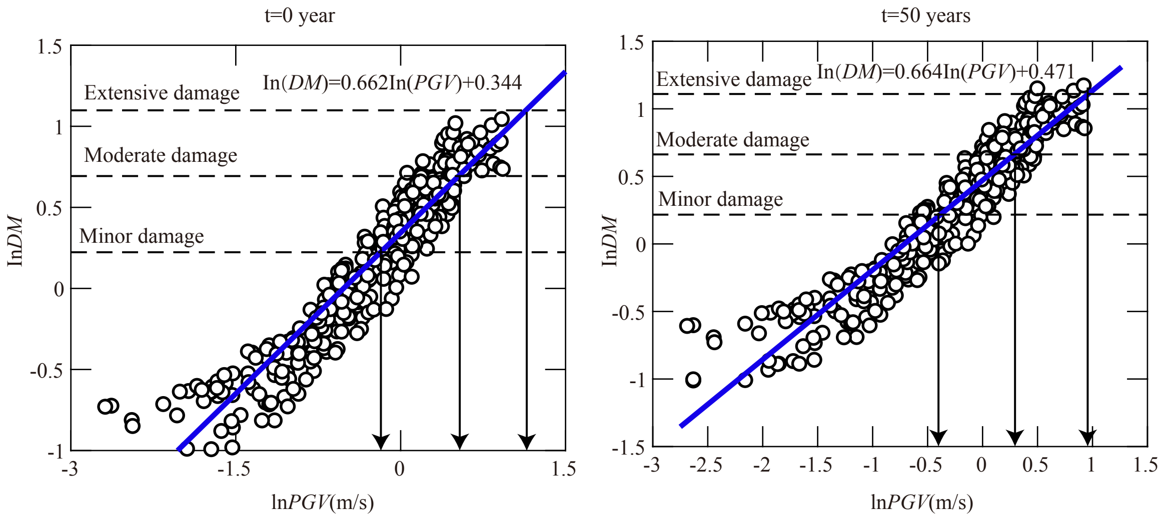

(b) Deep tunnel in soil type D

Fig.8. *DM – PGV* (in m/s) relationship for initial conditions (*t*=0 year) and for the aging scenario of 50 years. (a)Shallow tunnel in soil type D; (b) Deep tunnel in soil type D.

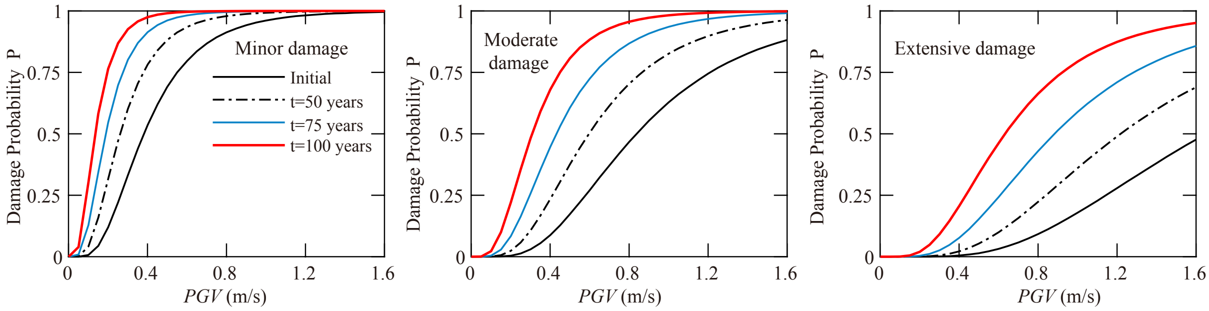

(a) Minor damage (b) Moderate damage (c) Extensive damage

Fig. 9. Fragility curves for shallow tunnel in soil type D. (a) Minor damage; (b) Moderate damage; (c) Extensive damage.

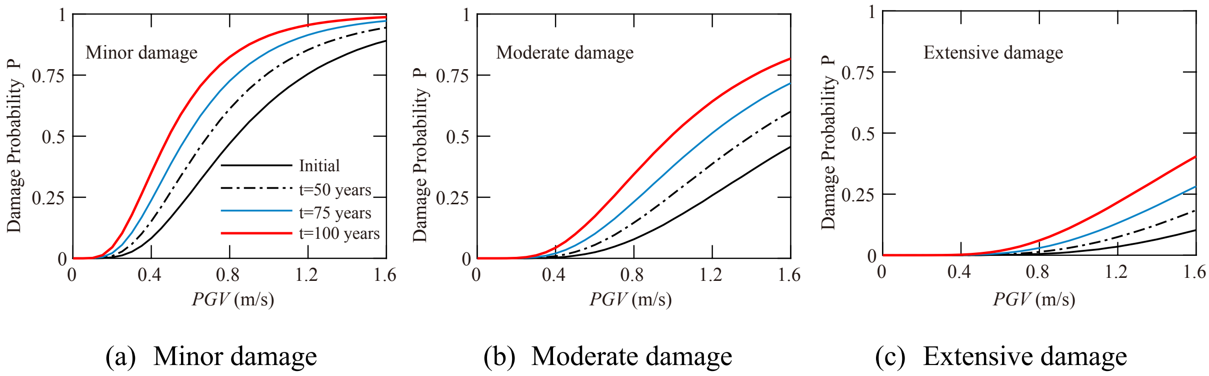

Fig. 10. Fragility curves for the deep tunnel in soil type D. (a) Minor damage; (b) Moderate damage; (c) Extensive damage.

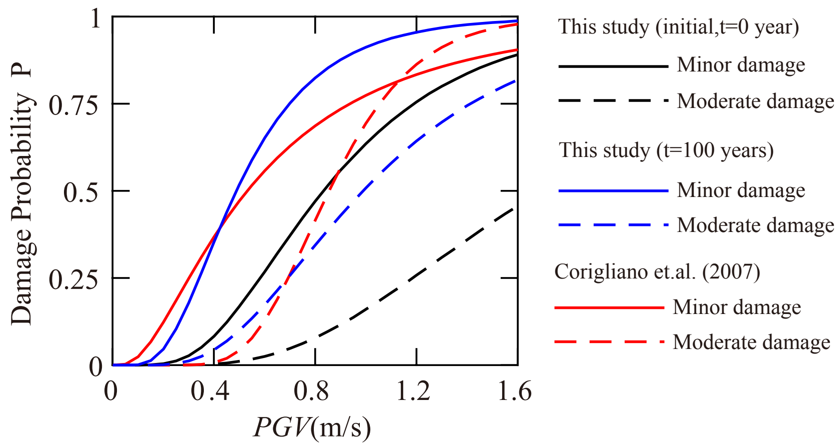

Fig. 11. Fragility curves for the deep tunnel in soil type D developed in this study and comparison with empirical ones by Corigliano et al. (2007).

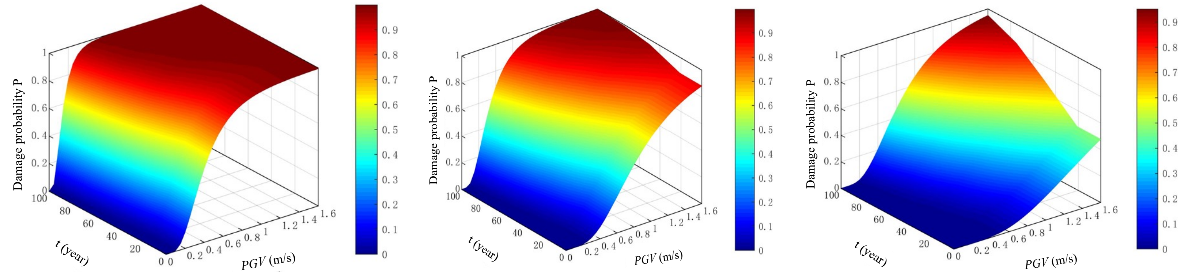

(a) Minor damage (b) Moderate damage (c) Extensive damage

Fig. 12. Fragility surfaces in terms of service time *t* and *PGV* for the shallow tunnel in soil type D.

(a) Minor damage; (b) Moderate damage;(c) Extensive damage.

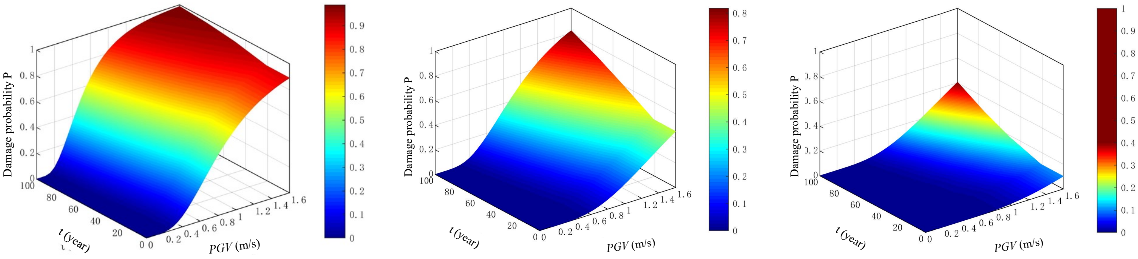

(a) Minor damage (b) Moderate damage (c) Extensive damage

Fig. 13. Fragility surfaces in terms of service time *t* and *PGV* for the deep tunnel in soil type D.

(a) Minor damage; (b) Moderate damage;(c) Extensive damage.